Contribution from the Laboratoire de Chimie Théorique, Université de Paris-Sud, 91405 Orsay, France, and Department of Chemistry, North Carolina State University, Raleigh, North Carolina 27695-8204

Band Electronic Structure Study of the Structural Modulation in the Magnéli Phase Mo_8O_{23}

Enric Canadell*,† and Myung-Hwan Whangbo*,‡

Received November 14, 1989

We examined the cause for the $0.5b^*$ superlattice modulation in the Magnéli phase Mo_8O_{23} by performing tight-binding band electronic structure calculations on Mo_8O_{23}, which consists of perovskite Mo_4O_{15} layers linked by Mo_4O_{14} chains. Our study shows that Mo_8O_{23} is a semimetal and does not possess a half-filled band dispersive along the b^* direction. Thus, the superlattice modulation is not caused by an electronic instability associated with Fermi surface nesting. The most likely cause for the superlattice modulation is a concerted pairwise rotation of MoO_6 octahedra in the perovskite Mo_4O_{15} layers.

Recently, a number of binary and ternary molybdenum oxides have been studied in connection with their low-dimensional metallic character and their associated physical properties.[1] For instance, ternary oxides, blue bronze $A_{0.3}MoO_3$ (A = K, Rb, Tl),[2] purple bronze $A_{0.9}Mo_6O_{17}$ (A = Li, Na, K, Tl),[3,4] and rare-earth bronze $La_2Mo_2O_7$[5] are all low-dimensional metals at room temperature and exhibit resistivity anomalies at low temperatures. Resistivity anomalies of low-dimensional metals are typically caused by the fact that their band electronic structures possess electronic instabilities originating from Fermi surface nesting. Thus, band electronic structure calculations[6] have become an indispensable tool in understanding the physical properties of molybdenum oxide metals.

Like the ternary oxide metals, binary oxide metal Mo_4O_{11} also shows a resistivity anomaly at low temperature.[7] This anomaly stems from a charge density wave (CDW) formation, as confirmed by the observation of diffuse spots in neutron and diffuse X-ray diffraction measurements.[7e] The observed CDW vector of Mo_4O_{11} is in excellent agreement with the nesting vector of the calculated Fermi surface for Mo_4O_{11}.[6e] The Magnéli phase Mo_4O_{11} is a member of the binary oxide family Mo_nO_{3n-1} (e.g., n = 4, 8, 9).[7,8] The Magnéli phase Mo_8O_{23} exhibits no superlattice spots above 360 K but shows incommensurate superlattice spots at q_{ic} = ($0.195a^*$, $0.5b^*$, $-0.120c^*$) between 360 and 285 K and commensurate superlattice spots at q_c = (0, $0.5b^*$, 0) below 285 K.[9] The presence of the $0.5b^*$ component shows that the unit cell size of Mo_8O_{23} doubles along the b-axis direction as the temperature is lowered below 360 K. According to the electronic instability argument based upon Fermi surface nesting, the $0.5b^*$ component implies that Mo_8O_{23} has a half-filled band primarily dispersive along the b^* direction (i.e., b direction). However, this is rather unlikely: According to the usual oxidation formalism of O^{2-}, Mo_8O_{23} has only two d electrons per formula unit to fill its 24 t_{2g}-block bands. Furthermore, the Magnéli phase Mo_9O_{26} also has two d electrons to fill its 27 t_{2g}-block bands, but it exhibits a superlattice modulation with a $0.5b^*$ component.[10] In the present work, we show that the structural modulation of Mo_8O_{23} does not originate from an electronic instability associated with Fermi surface nesting by performing tight-binding band calculations[11] on Mo_8O_{23} on the basis of its crystal structure determined at 370 K. The atomic parameters employed in constructing our extended Hückel[12] tight-binding Hamiltonian are identical with those used in our previous studies[6] on binary and ternary molybdenum oxides.

Crystal Structure

To describe the nature of the partially filled d-block bands of Mo_8O_{23}, which primarily govern its electronic properties, it is necessary to examine the crystal structure in some detail. The ideal structural pattern of Mo_8O_{23} can be described in terms of regular MoO_6 octahedra as follows: The MoO_5 chain **1** is obtained from MoO_6 octahedra upon sharing their axial oxygen (O_{ax}) atoms. Provided that the projection view of **1** along the chain is given by **2**, the projection view **3** represents an Mo_4O_{14} quadruple

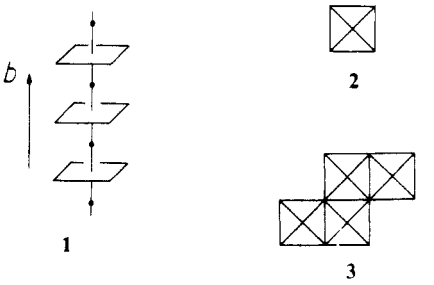

† Université de Paris-Sud.
‡ North Carolina State University.

(1) Recent reviews: (a) Greenblatt, M. *Chem. Rev.* **1988**, *88*, 31. (b) Schlenker, C., Ed. *Low-Dimensional Properties of Molybdenum Bronzes and Oxides*; Reidel: Dordrecht, The Netherlands, 1989. (c) Whangbo, M.-H.; Canadell, E. *Acc. Chem. Res.* **1989**, *22*, 375.
(2) (a) Ghedira, M.; Chenavas, J.; Marezio, M.; Marcus, J. *J. Solid State Chem.* **1985**, *57*, 300. (b) Ganne, M.; Boumaza, A.; Dion, M.; Dumas, J. *Mater. Res. Bull.* **1985**, *20*, 1297. (c) Graham, J.; Wadsley, A. D. *Acta Crystallogr.* **1966**, *20*, 93. (d) Pouget, J. P.; Kagoshima, S.; Schlenker, C.; Marcus, J. *J. Phys. Lett.* **1983**, *44*, L133. (e) Fleming, R.; Schneemeyer, L. F.; Moncton, D. E. *Phys. Rev. B.* **1985**, *31*, 899. (f) Tamegai, T.; Tsutsumi, K.; Kagoshima, S.; Kanai, Y.; Taui, M.; Tomozawa, H.; Sato, M.; Tsuji, K.; Harada, J.; Sakata, M.; Nakajima, T. *Solid State Commun.* **1984**, *51*, 585. (g) Pouget, J. P.; Noguera, C.; Moudden, A. H.; Moret, T. *J. Phys.* (*Les Ulis., Fr.*) **1985**, *46*, 1731.
(3) (a) Vincent, H.; Ghedira, M.; Marcus, J.; Mercier, J.; Schlenker, C. *J. Solid State Chem.* **1983**, *47*, 113. (b) Greenblatt, M.; Ramanujachary, K. V.; McCarroll, W. H.; Neifeld, R.; Waszczak, J. V. *J. Solid State Chem.* **1985**, *59*, 149. (c) Ganne, M.; Dion, M.; Boumaza, A.; Tournoux, M. *Solid State Commun.* **1986**, *59*, 137. (d) Ramanujachary, K. V.; Collins, B. T.; Greenblatt, M. *Solid State Commun.* **1986**, *59*, 647. (e) Escribe-Filippini, C.; Konate, K.; Marcus, J.; Schlenker, C.; Almairac, R.; Ayroles, R.; Roucau, C. *Philos. Mag. B* **1984**, *50*, 321.
(4) (a) Onoda, M.; Toriumi, K.; Matsuda, Y.; Sato, M. *J. Solid State Chem.* **1987**, *66*, 163. (b) Greenblatt, M.; McCarroll, W. H.; Neifeld, R.; Croft, M.; Waszczak, J. V. *Solid State Commun.* **1984**, *51*, 671. (c) Schlenker, C.; Schwen, K. H.; Escribe-Filippini, C.; Marcus, J. *Physica* **1985**, *135B*, 511. (d) Matsuda, Y.; Onoda, M.; Sato, M. *Physica* **1986**, *143B*, 243.
(5) (a) Moioni, A.; Subramanian, M.; Clearfield, A.; DiSalvo, F. J.; McCarroll, W. H. *J. Solid State Chem.* **1987**, *66*, 136. (b) Collins, B. T.; Greenblatt, M.; McCarroll, W. H.; Hull, G. W. *J. Solid State Chem.* **1988**, *73*, 507.
(6) (a) Whangbo, M.-H.; Schneemeyer, L. F. *Inorg. Chem.* **1986**, *25*, 2424. (b) Whangbo, M.-H.; Canadell, E.; Schlenker, C. *J. Am. Chem. Soc.* **1987**, *109*, 6308. (c) Whangbo, M.-H.; Canadell, E. *J. Am. Chem. Soc.* **1988**, *110*, 358. (d) Whangbo, M.-H.; Canadell, E. *Inorg. Chem.* **1987**, *26*, 842. (e) Canadell, E.; Whangbo, M.-H.; Schlenker, C.; Escribe-Filippini, C. *Inorg. Chem.* **1989**, *28*, 1466.
(7) (a) Ghedira, M.; Vincent, H.; Marezio, M.; Marcus, J.; Fourcadot, G. *J. Solid State Chem.* **1985**, *56*, 66. (b) Kihlborg, L. *Arkiv. Kemi* **1963**, *21*, 365. (c) Magnéli, A. *Acta Chem. Scand.* **1948**, *2*, 861. (d) Schlenker, C.; Dumas, J. *Crystal Structures and Properties of Materials with Quasi-One-Dimensional Structures*; Rouxel, J., Ed.; Reidel: Dordrecht, The Netherlands, 1986; p 135. (e) Guyot, H.; Schlenker, C.; Pouget, J. P.; Ayroles, R.; Roucau, C. *J. Phys. C* **1985**, *18*, 427. (f) Guyot, H.; Schlenker, C.; Fourcadot, G.; Konate, K. *Solid State Commun.* **1985**, *54*, 909. (g) Guyot, H.; Escribe-Filippini, C.; Fourcadot, G.; Konate, K.; Schlenker, C. *J. Phys. C.* **1983**, *16*, L1227.
(8) Magnéli, A. *Acta Chem. Scand.* **1948**, *2*, 501.
(9) (a) Fujishita, H.; Sato, M.; Sato, S.; Hoshino, S. *J. Solid State Chem.* **1987**, *66*, 40. (b) Sato, M.; Fujishita, H.; Sato, S.; Hoshino, S. *J. Phys. C.* **1986**, *19*, 3059.

0020-1669/90/1329-2256$02.50/0

chain made up of four MoO_5 chains by sharing the equatorial oxygen (O_{eq}) atoms. In a similar manner, the projection view of Mo_8O_{23} along the *b* axis is given by **4**, which shows Mo_4O_{15} slabs

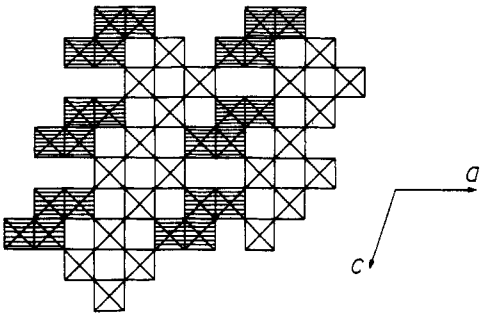

4

5 linked by the Mo_4O_{14} chains **3**. The Mo_4O_{15} slab **5** can be built

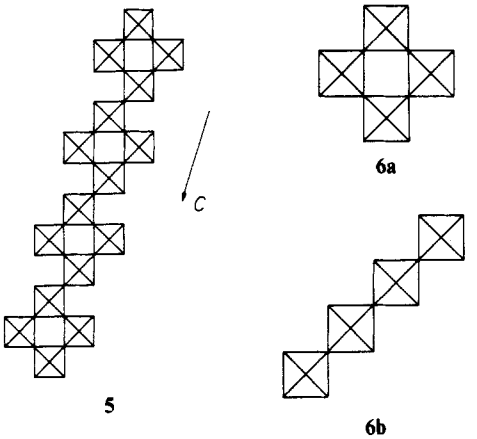

5

6a

6b

from the Mo_4O_{16} quadruple chains **6a**. All the MoO_6 octahedra of the Mo_4O_{15} slab are condensed by sharing their corners, so that the Mo_4O_{15} slab has a perovskite structure. The Mo_4O_{15} slab can also be considered as a stepped layer built from the Mo_4O_{17} chains **6b**. The Magnéli phase Mo_9O_{26} contains the stepped layer Mo_5O_{18} (**7**), which is built from the Mo_5O_{21} quintuple chains **8**. In the

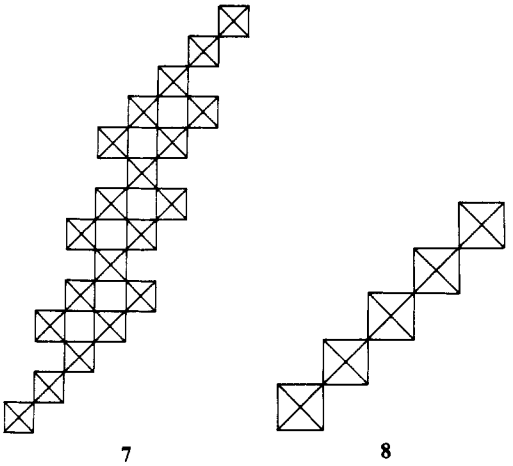

7

8

Magnéli phase Mo_9O_{26}, the Mo_5O_{18} layers are linked by the Mo_4O_{14} chains as in **4**.

The crystal structure of Mo_8O_{23} determined at 370 K (i.e., the crystal structure without superlattice modulation) shows[9a] that the MoO_6 octahedra are all distorted from an ideal, regular octahedron. Every MoO_6 octahedron of Mo_8O_{23} shows a strong O–Mo···O bond alternation (e.g., Mo–O = 1.69 Å and Mo···O = 2.37 Å) along the *b* axis. Every Mo atom of MoO_6 is located slightly out of the four O_{eq} atom plane, as depicted in **9**, where

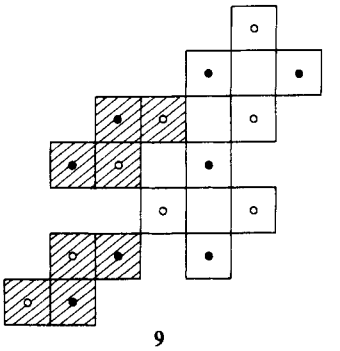

9

the filled and empty circles represent the Mo atoms lying above and below the four O_{eq} atom planes, respectively. The senses of O–Mo···O alternation at these two kinds of Mo atoms are opposite (i.e., O–Mo···O at one and O···Mo–O at the other) so that the unit cell of Mo_8O_{23} is given by $(Mo_8O_{23})_2$.

The Mo–O bonds associated with the O_{eq} atoms of the Mo_4O_{14} chains **3** and the Mo_4O_{15} slabs **5** are shown in **10** and **11**, respectively. Note that every MoO_6 octahedron of the Mo_4O_{14} chain **3** has one short Mo–O_{eq} bond (less than 1.80 Å), while that of the Mo_4O_{15} slab has Mo–O_{eq} bonds longer than 1.82 Å. Simply speaking, therefore, the MoO_6 octahedra of the Mo_4O_{15} slab **5** have a distortion in which one Mo–O bond is shortened, and those of the Mo_4O_{14} chains **3** have a distortion in which two Mo–O bonds are shortened. This difference in the octahedral distortions has an important consequence upon the electronic properties of Mo_8O_{23}, as will be shown in the following.

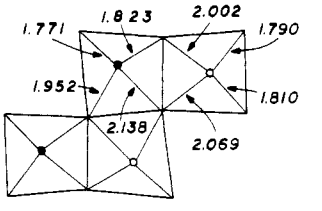

10

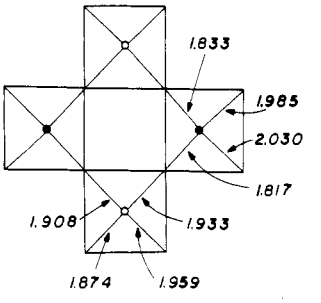

11

Band Electronic Structure

A. Octahedral Distortion and t_{2g}-Block Level Splitting. As depicted in **12a**, shortening of one Mo–O bond raises two π-type

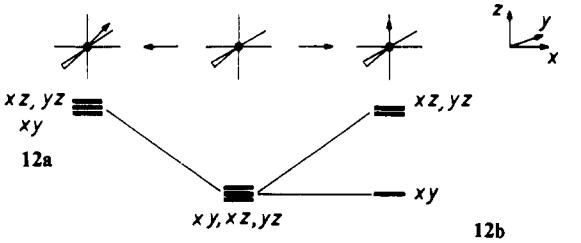

12a **12b**

(10) Onoda, M.; Fujishita, H.; Matsuda, Y.; Sato, M. *Synth. Met.* **1987**, *19*, 947.
(11) Whangbo, M.-H.; Hoffmann, R. *J. Am. Chem. Soc.* **1978**, *100*, 6093.
(12) Hoffmann, R. *J. Chem. Phys.* **1963**, *39*, 1397. A modified Wolfsberg–Helmholz formula was used to calculate the off-diagonal H_{ij} values: Ammeter, J. H.; Bürgi, H.-B.; Thibeault, J.; Hoffmann, R. *J. Am. Chem. Soc.* **1978**, *100*, 3686.

t_{2g}-block levels (i.e., *xz* and *yz*) leaving behind one δ-type t_{2g}-block level (i.e., *xy*). (Here the δ and π levels are classified with respect to the shortened Mo–O bond.)[1c,13] When an octahedral distortion shortens two cis Mo–O bonds, all three t_{2g}-block levels are raised in energy as shown in **12b**. For a molybdenum oxide lattice consisting of distorted MoO_6 octahedra, the lowest lying d-block bands originate from the octahedra with the lowest lying t_{2g}-block level. As discussed in the previous section, Mo_8O_{23} contains MoO_6 octahedra with one short Mo–O bond (in the Mo_4O_{15} slabs **5**) and those with two short Mo–O bonds (in the Mo_4O_{14} chains **3**). Therefore, it is expected that the lowest lying d-block bands of Mo_8O_{23} represent the Mo_4O_{15} slabs, and only those bands are occupied because of the very low d-electron count in Mo_8O_{23}.

B. t_{2g}-Block Bands of the Mo_4O_{15} Slab and the Mo_4O_{14} Chain. To examine the effects of the O–Mo···O alternation upon band electronic structure, we consider an ideal MoO_5 chain **2** constructed from regular MoO_6 octahedra with Mo–O = 1.956 Å (i.e., the average Mo–O distance) and also a model MoO_5 chain **2** with the O–Mo···O bond alternation of Mo–O = 1.656 Å and Mo···O = 2.256 Å along the chain and with the Mo atom displaced from the four O_{eq} atom plane along the chain direction by 0.3 Å. Parts a and b of Figure 1 show the t_{2g}-block bands calculated for the ideal and the model MoO_5 chains, respectively. Clearly, the O–Mo···O alternation raises the doubly degenerate π bands above the δ band. Figure 1c shows the t_{2g}-block bands of the Mo_4O_{16} chain **6a** constructed from four model MoO_5 chains mentioned above. The four flat bands a–d of Figure 1c are δ bands. Band a has the nodal property **13a**, bands b and c (degenerate) have the nodal properties **13b** and **13c**, respectively, and band d has the nodal property **13d**. Band a of Figure 1c lies lower in energy than the bottom band of Figure 1b, since the shared O_{eq} corners of **3** do not have oxygen p-oribital contribution in **13a** by symmetry.

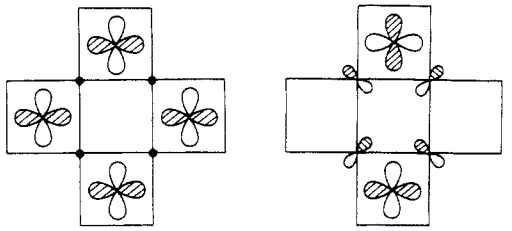

13a **13b**

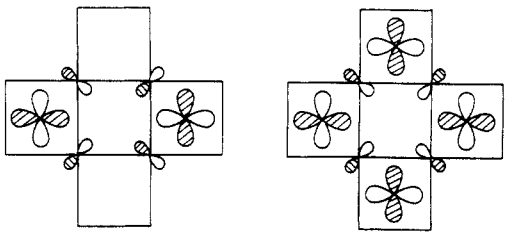

13c **13d**

Figure 2a shows the bottom three (δ type) of the t_{2g}-block bands calculated for the real Mo_4O_{16} chain **6a** taken from the crystal structure of Mo_8O_{23}. The degeneracy between bands b and c is lifted due to the lowering of symmetry in the crystal structure. Figure 2b shows the bottom portion of the t_{2g}-block bands calculated for the real Mo_4O_{15} slab [with the unit cell formula of $(Mo_4O_{15})_2$] taken from the crystal structure of Mo_8O_{23}. Bands a_1 and a_2 (b_1 and b_2) of Figure 2b have the orbital character of band a (b) of Figure 2a. Bands a_1 and a_2 are dispersive along the c^* direction, and so are bands b_1 and b_2, because the δ orbital (with respect to the *b* axis) at each MoO_6 octahedron is engaged in π-type interactions along the *c*-axis direction. For example,

(13) (a) Whangbo, M.-H.; Evain, M.; Canadell, E.; Ganne, M. *Inorg. Chem.* **1989**, *28*, 267. (b) Canadell, E.; Whangbo, M.-H. *Inorg. Chem.* **1988**, *27*, 288.

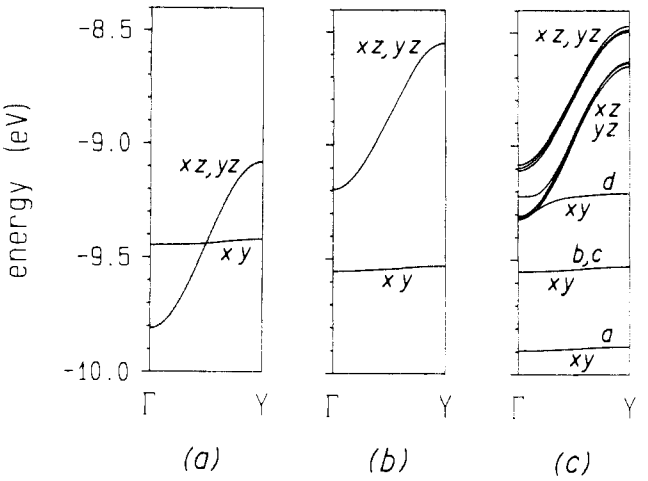

Figure 1. Dispersion relations of the t_{2g}-block bands calculated for (a) the ideal MoO_5 chain **2**, (b) the model MoO_5 chain **2** with O–Mo···O alternation, and (c) the model Mo_4O_{16} chain **6a** with O–Mo···O alternation. $\Gamma = 0$, and $Y = b^*/2$.

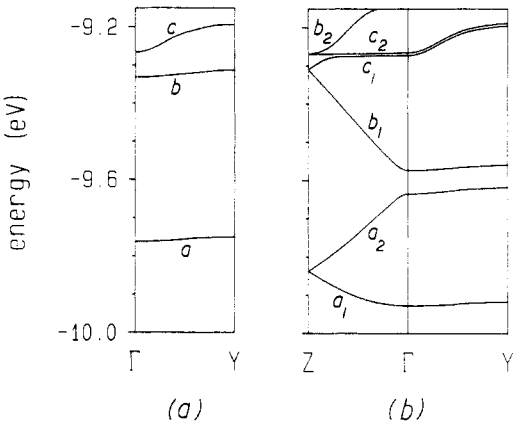

Figure 2. Dispersion relations for the bottom portion of the t_{2g}-block bands calculated for (a) the real Mo_4O_{16} chain **6a** and (b) the real Mo_4O_{15} slab **5**. In (b), $\Gamma = (0, 0)$, $Y = (b^*/2, 0)$, and $Z = (0, c^*/2)$.

the nodal properties of bands a_1 and a_2 at Γ are given by **14a** and **14b**, respectively, and those of bands b_1 and b_2 at Γ by **15a** and

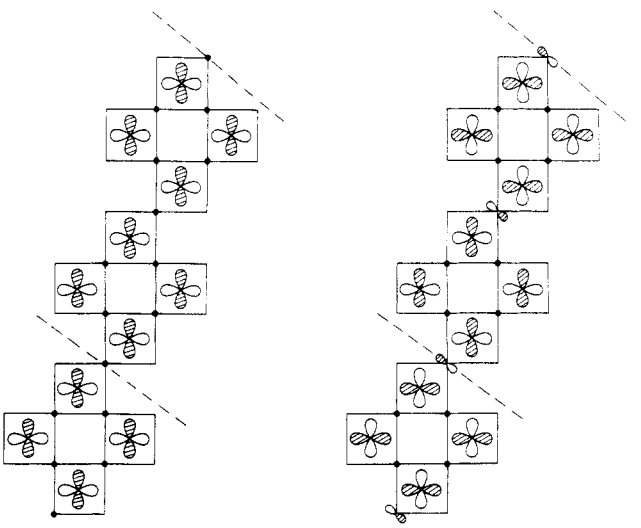

14a **14b**

15b, respectively. Bands c_1 and c_2 are not dispersive along the c^* direction, since the unit cell orbital **13c** practically does not have any orbital contribution at the shared O_{eq} atoms (between

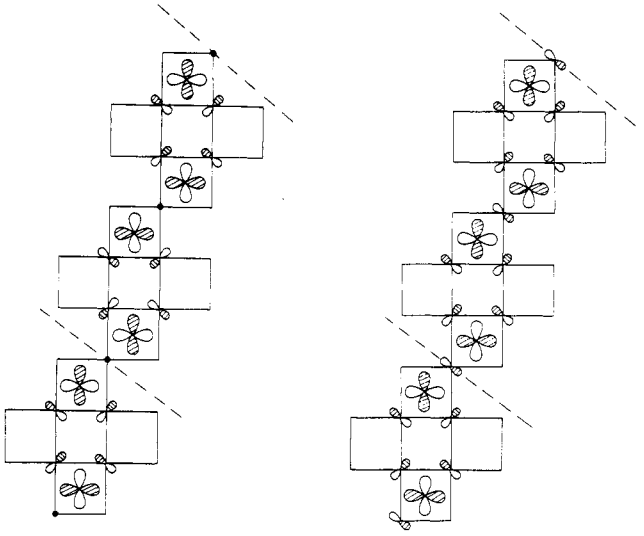

15a **15b**

unit cells). This is shown by **16a** and **16b**, which are the nodal

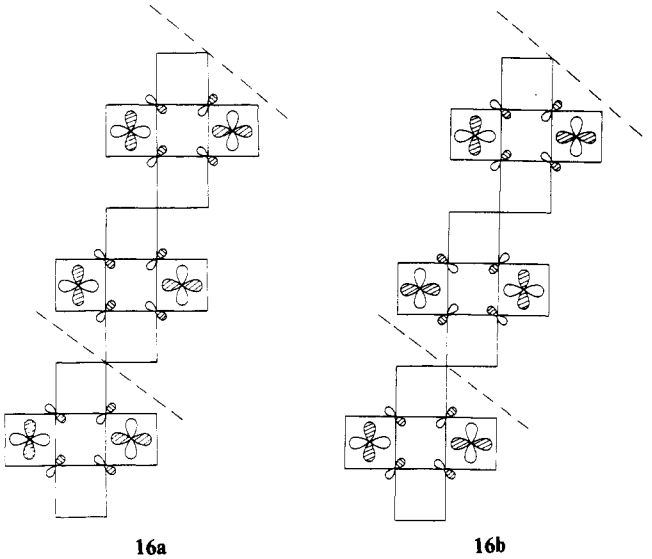

16a **16b**

properties of bands c_1 and c_2 at Γ, respectively. Bands a_1 and a_2 merge at Z, since by the changing of the relative phases between adjacent unit cells, band a_1 picks up but band a_2 removes the oxygen p-orbital contribution from the shared O_{eq} atoms between unit cells. Similarly, bands b_1 and b_2 merge at Z and so do bands c_1 and c_2.

Figure 3 shows the bottom portion of the t_{2g}-block bands calculated for the real Mo_4O_{14} quadruple chain **3** taken from the crystal structure of Mo_8O_{23}. With respect to the bottom bands of Mo_4O_{15} slab shown in Figure 2b, all d-block bands of the Mo_4O_{14} chain are substantially raised in energy. This reflects the fact that the t_{2g}-block levels of the MoO_6 octahedra in the Mo_4O_{14} chain are higher lying in energy because those octahedra have two short Mo–O bonds.

C. t_{2g}-Block Bands of Mo_8O_{23}. If there is no appreciable interaction between the Mo_4O_{15} slabs and the Mo_4O_{14} chains in Mo_8O_{23}, superposition of Figures 2b and 3 would be a good approximation for the t_{2g}-block bands of Mo_8O_{23}. With four d electrons per unit cell $(Mo_8O_{23})_2$, it is expected that only bands a_1 and a_2 of the Mo_4O_{15} slabs are occupied and all d-block bands of the Mo_4O_{14} chains are unoccupied. Figure 4 shows the bottom portion of the t_{2g}-block bands calculated for the three-dimensional lattice of Mo_8O_{23}. As anticipated, these bands are essentially represented by the Mo_4O_{15} slabs. The t_{2g}-block bands representing the Mo_4O_{14} chains lie well above the bands shown in Figure 4. Bands a_2 and b_1 are separated by a small band gap in an isolated Mo_4O_{15} slab (Figure 2b) but overlap in a semimetallic manner in Mo_8O_{23} (Figure 4).

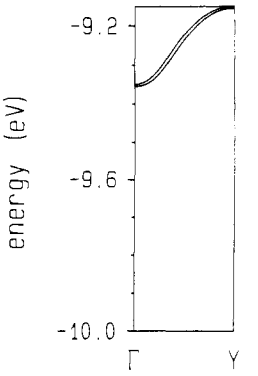

Figure 3. Dispersion relations for the bottom portion of the t_{2g}-block, bands calculated for the real Mo_4O_{14} chain **3**.

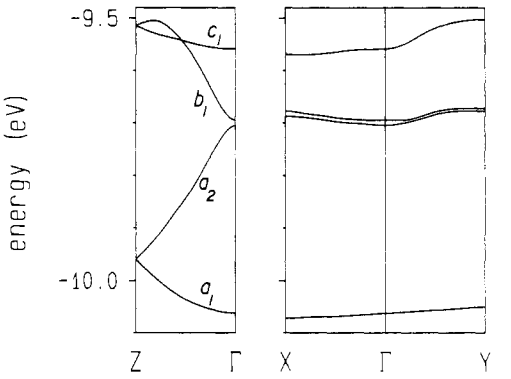

Figure 4. Dispersion relations for the bottom portion of the d-block bands calculated for Mo_8O_{23}. Γ = (0, 0, 0), $X = (a^*/2, 0, 0)$, $Y = (0, b^*/2, 0)$, and $Z = (0, 0, c^*/2)$.

There are two important observations to note from Figure 4: (a) Mo_8O_{23} is predicted to be a semimetal and does not have a half-filled band dispersive along the b^* direction. All the bands of Figure 4 are not dispersive along the b^* direction, since they are largely based upon δ orbitals with respect to the b axis. (b) Only the bottom d-block bands of the Mo_4O_{15} slabs are filled, while the d-block bands of the Mo_4O_{14} chains are empty. Consequently, the Mo atoms of the Mo_4O_{15} slabs should be lower in their formal oxidation states than those of the Mo_4O_{14} chains (i.e., approximately, $Mo^{5.5+}$ for the Mo_4O_{15} slabs and Mo^{6+} for the Mo_4O_{14} chains). Zachariasen analysis[14] for Mo_8O_{23} leads to an unreasonable result, since it predicts that all Mo atoms are nearly the same in their oxidation states (i.e., approximately $Mo^{5.75+}$).[10]

Superlattice Modulation

Our study shows that the Magnêli phase Mo_8O_{23} is a semimetal and has two partially filled bands resulting primarily from its structural components Mo_4O_{15} slabs. These two bands are not dispersive along the b^* and a^* directions but dispersive along the c^* direction. Namely, Mo_8O_{23} does not possess a half-filled band dispersive along the b^* direction, so that the $0.5b^*$ component of the superlattice modulation in Mo_8O_{23} does not originate from an electronic instability associated with Fermi surface nesting. As suggested by Pouget,[15] therefore, the cause for the $0.5b^*$ modulation is likely to be the well-known structural instability inherent in perovskite metal oxides, i.e., the concerted pairwise rotations of MO_6 octahedra within a layer of corner-shared MO_6 octahedra.[16] As illustrated in **17** for an Mo_4O_{17} quadruple chain **6b** (see also **4** and **5**), rotation of an MoO_6 octahedron around an O–Mo–O axis (perpendicular to the chain direction b axis)

(14) Zachariasen, W. H. *J. Less-Common Met.* **1978**, *62*, 1.
(15) Pouget, J. P. Reference 1b, p 87.
(16) (a) Shirane, G.; Yamada, Y. *Phys. Rev.* **1969**, *177*, 858. (b) Fuji, Y.; Hoshino, S.; Yamada, Y.; Shirane, G. *Phys. Rev. B* **1974**, *9*, 4549. (c) Sato, M.; Grier, B. H.; Shirane, G.; Akahane, T. *Phys. Rev. B* **1982**, *25*, 6876.

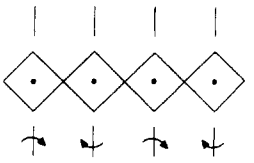

17

induces a concerted pairwise rotation of all MoO_6 octahedra within the Mo_4O_{17} chain. This doubles the unit cell size along the b direction and accounts for the $0.5b^*$ component. Indeed, the crystal structure of Mo_8O_{23} determined at 100 K[9a] and the inelatic neutron scattering data[17] of Mo_8O_{23} are consistent with the concerted pairwise octahedral rotation described above. We expect that the $0.5b^*$ structural modulation observed for Mo_9O_{26} is also caused by the same mechanism.

We now discuss how the concerted pairwise rotations of the Mo_4O_{17} chains can correlate with the commensurate and incommensurate modulations of the Mo_4O_{15} slab and eventually the Mo_8O_{23} lattice. The senses of the concerted rotations of adjacent Mo_4O_{17} chains can be identical (the M_3 type mode shown in **18a**) or opposite (the R_{25} type mode shown in **18b**).[16c] As shown in

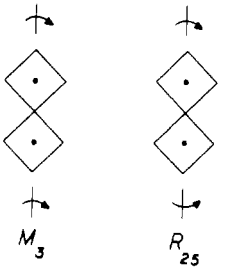

18a **18b**

Figure 5, the unmodulated Mo_4O_{15} slab has several symmetry elements, i.e., the center of inversion, the 2-fold rotation, and the glide planes at $y = 0$ and $^1/_2$. The M_3 or R_{25} mode of rotation lowers the symmetry of the lattice, so that the symmetry elements of the unmodulated structure may become incompatible with the superlattice modulation. As pointed out earlier, the senses of the O–Mo···O alterations in adjacent MoO_5 octahedral chains of each Mo_4O_{17} chain are opposite (see **9** and the text). Because of this geometrical aspect, it can be shown that the commensurate superlattice modulation $q_c = (0, 0.5b^*, 0)$ is compatible with the presence of (a) the 2-fold rotation for the M_3 mode of rotation, (b) the glide plane at $y = 0$ for the R_{25} mode of rotation, and (c) the glide plane at $y = ^1/_2$ for the M_3 mode of rotation. For the commensurate superlattice modulation, the rotational angles a–d are identical with a″–d″, respectively (Figure 5). Case c considered above does not place any constraining relationship among the angles a–d, among a′–d′, or between a–d and a′–d′. This is not true with cases a and b. For instance, condition a means that a = d, b = c, a′ = d′, and b′ = c′. Therefore, case c is expected to induce less lattice strain than case a or b. Therefore, it is not surprising that case c is the one observed for the commensurate superlattice modulation of Mo_8O_{23}. An incommensurate superlattice modulation of an Mo_4O_{15} slab along the c direction implies that the variation of the ratios of successive rotational angles a/c, a″/c″, etc. (see Figure 5) follows an incommensurate wave pattern. The Mo_4O_{15} slabs are linked by the Mo_4O_{14} chains (see **3** and **4**), so that the incommensurate modulation of an Mo_4O_{15} slab would cause different amounts of strain on the successive Mo_4O_{14} chains. This might cause an incommensurate modulation in the Mo_8O_{23} lattice along the a direction.

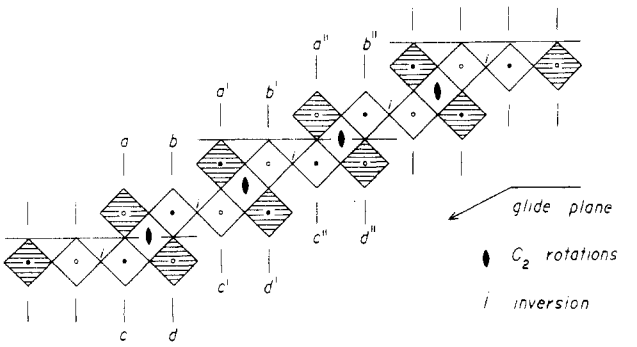

Figure 5. Schematic diagram of the unmodulated Mo_4O_{15} slab, showing the symmetry elements and the octahedral rotational angles (a–d, a′–d′, and a″–d″). The thin horizontal lines distinguish successive unit cells, and the thick vertical lines refer to the rotational axes. The shaded octahedra are equivalent, and so are the unshaded octahedra. The filled and empty circles of octahedra signify that the senses of the O–Mo···O alternations along the b axis are opposite.

Concluding Remarks

The two partially filled bands of Mo_8O_{23} are nearly flat along the b^* direction, since they are constructed from the δ orbitals of MoO_6 octahedra with respect to the b axis. These bands are nearly flat along the a^* axis as well, since interactions between the Mo_4O_{15} slabs in Mo_8O_{23} occur indirectly via the Mo_4O_{14} chains (see **5**), whose d-block levels lie well above the δ orbitals of the Mo_4O_{15} slabs. Along the c^* direction, however, the two partially filled bands of Mo_8O_{23} are dispersive because the δ orbitals make π-type interactions along the c direction (see **14** and **15**). This explains why Mo_8O_{23} does not have a half-filled band dispersive along the b^* direction and hence why its $0.5b^*$ superlattice modulation does not originate from an electronic instability associated with Fermi surface nesting. The most likely cause for the superlattice modulation would be the concerted pairwise rotation of MoO_6 octahedra in the perovskite slabs Mo_4O_{15}, as pointed out by Pouget.[15] The anisotropic band dispersions of Mo_8O_{23} also suggest that the electrical resistivities ρ along the a^*, b, and c directions would vary as $\rho_c \ll \rho_{a^*} < \rho_b$. This prediction, though based upon the crystal structure of Mo_8O_{23} determined at 370 K, would be valid for temperatures below room temperature, since the slight octahedral rotations in the Mo_4O_{15} slabs are not expected to change the essential features of the Mo_8O_{23} electronic structure described above. For example, the band electronic structures calculated for the real Mo_4O_{16} chain **6a** and the real Mo_4O_{14} chain **3**, taken from the crystal structure of Mo_8O_{23} determined at 100 K, are very similar to those calculated for the corresponding chains without structural modulation (i.e., those in Figures 2a and 3, respectively) except that each band of the unmodulated structure splits into two bands with small energy difference by the structural modulation. Surprisingly, the available experimental data[18] determined below room temperature show that $\rho_{a^*} < \rho_c < \rho_b$. Further studies are necessary to resolve the difference between theory and experiment concerning the relative magnitudes of ρ_{a^*} and ρ_c in Mo_8O_{23}.

Acknowledgment. This work was supported by NATO, Scientific Affairs Division, and also by DOE, Office of Basic Sciences, Division of Materials Sciences, under Grant DE-FG05-86ER45259. We express our appreciation for computing time on the ER-Cray computer made available by DOE.

(17) Fujishita, H.; Sato, M.; Shapiro, S. M.; Hoshino, S. *Physica B* **1986**, *143*, 201.

(18) (a) Sato, M.; Nakao, K.; Hoshino, S. *J. Phys. C* **1984**, *17*, L817. (b) Gruber, H.; Krautz, E.; Fritzer, H. P.; Gatterer, K.; Popitsch, A. *Solid State Commum.* **1986**, *58*, 133.